

DeepScan: A Training-Free Framework for Visually Grounded Reasoning in Large Vision-Language Models

Yangfu Li^{*} Hongjian Zhan^{*,*} Jiawei Chen^{*} Yuning Gong^{♡,◇} Qi Liu^{*} Yue Lu^{*}

^{*}East China Normal University, [♡]Sichuan University, [◇]Shanghai AI Laboratory

{yfli.cee, qiliu}@stu.ecnu.edu.cn, hjzhan@cee.ecnu.edu.cn, ylu@cs.ecnu.edu.cn

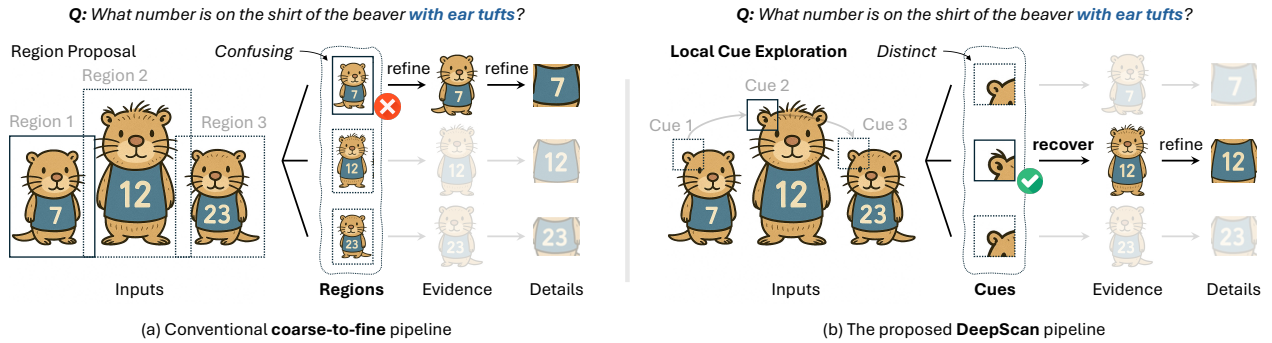


Figure 1. Comparison of grounding pipelines in existing methods and the proposed DeepScan. (a) Existing methods depend on *one-shot* localization of evidence regions, making them sensitive to noisy contexts. (b) DeepScan uses local cue exploration to identify discriminative cues and recovers evidence from these cues in a *bottom-up* manner, robustly localizing critical visual content even in challenging scenes.

Abstract

Humans can robustly localize visual evidence and provide grounded answers even in noisy environments by identifying critical cues and then relating them to the full context in a bottom-up manner. Inspired by this, we propose DeepScan, a training-free framework that combines Hierarchical Scanning, Refocusing, and Evidence-Enhanced Reasoning for visually grounded reasoning in Large Vision-Language Models (LVLMs). Unlike existing methods that pursue one-shot localization of complete evidence, Hierarchical Scanning performs local cue exploration and multi-scale evidence extraction to recover evidence in a bottom-up manner, effectively mitigating the impacts of distractive context. Refocusing then optimizes the localized evidence view through collaboration of LVLMs and visual experts. Finally, Evidence-Enhanced Reasoning aggregates multi-granular views via a hybrid evidence memory and yields accurate and interpretable answers. Experimental results demonstrate that DeepScan significantly boosts LVLMs in diverse visual tasks, especially in fine-grained visual understanding. It achieves 90.6% overall accuracy on V* when integrated with Qwen2.5-VL-7B. Moreover, DeepScan provides consistent improvements for LVLMs across various architectures and model scales without additional adaptation cost. The code will be open-source at [DeepScan](#).

^{*}Corresponding Author. This work is accepted to CVPR'26.

1. Introduction

Humans excel at grounding critical visual information and reasoning based on the located evidence, which is a hallmark of intelligence recognized in the cognitive and vision science. [38, 40, 41]. While this is natural to humans, it remains challenging for Large Vision-Language Models (LVLMs) to replicate this behavior, leading to suboptimal performance in complex visual tasks [16, 34, 39, 42].

To reproduce this ability in LVLMs, some approaches have employed reinforcement learning [31, 35, 50, 52] with visually supervised rewards (e.g., IoU) or context engineering [42, 46], enabling active perception and localization of evidence during reasoning. Another line of research augments LVLM grounding with auxiliary modules [4, 26, 45, 51]. More recently, several studies [2, 13, 24] integrate external visual experts, such as GroundingDINO [20, 27] and LangSAM [21], to localize visual evidence based on the consensus between these experts and LVLMs, significantly enhancing fine-grained visual understanding in LVLMs.

Despite these advances, most existing methods follow a *top-down* grounding paradigm: they first perform an image-level search for coarse-grained proxies, such as region proposals [31, 35, 46, 50, 52], detection boxes [13, 24], or textual descriptions [39], and then refine these proxies to obtain fine-grained evidence. However, this paradigm requires the *one-shot* localization of complete evidence regions from

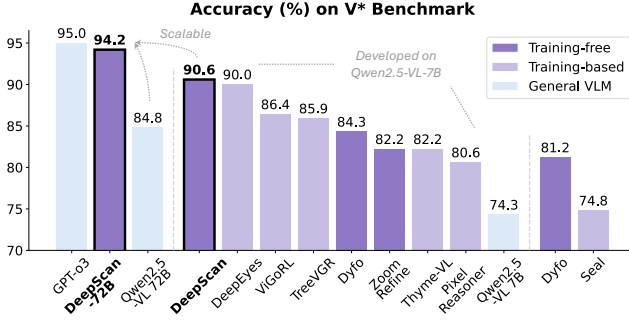


Figure 2. Performance of LVLMs and visually grounded reasoning variants on V*. DeepScan achieves highly competitive results.

the entire image, which is easily affected by noisy context, *i.e.*, attention sink [43], or semantically similar objects, *i.e.*, attention drift [6], leading to suboptimal performance. In such cases, the LVLM either refuses to answer or makes uninformed guesses based on incorrect evidence, as illustrated in Fig. 1. By contrast, humans intuitively adopt a *bottom-up* routine in challenging visual tasks. For example, when playing the “*spot-the-difference*” puzzles, people scan local patches for subtle discrepancies within largely similar content, then verify these cues at the image level to recover the target while suppressing distracting context.

Inspired by this human behavior, we propose **DeepScan**, a training-free framework for visually grounded reasoning in LVLMs, comprising Hierarchical Scanning, Refocusing, and Evidence-Enhanced Reasoning. Unlike existing methods, Hierarchical Scanning leverages patch-wise cue exploration and image-level evidence extraction to robustly localize visual evidence in a bottom-up manner. Refocusing further refines the surrounding context of the extracted evidence through collaboration between the visual experts and LVLMs, reducing information loss. Finally, Evidence-Enhanced Reasoning utilizes a Hybrid Evidence Memory to provide LVLMs with multi-granular evidence views, producing accurate and well-grounded answers. Fig. 2 shows that DeepScan performs competitively with leading approaches. Moreover, as a training-free framework, DeepScan scales seamlessly to larger models (*e.g.*, Qwen2.5-VL-72B), yielding consistently improved performance. Extensive experiments across diverse visual tasks further demonstrate its effectiveness. Our contributions are fourfold:

- ❶ We introduce **DeepScan**, a training-free framework that boosts LVLM performance by explicitly localizing, recalibrating, and integrating evidence before answering.
- ❷ We propose **Hierarchical Scanning**, a bottom-up visual grounding paradigm that mitigates noisy context via local cue exploration and multi-scale evidence extraction.
- ❸ We present **Refocusing**, a collaborative search paradigm that recalibrates the evidence view through interactions between LVLMs and external visual experts.

- ❹ Comprehensive experiments validate the superiority of DeepScan. It provides average improvements of 16.3% on V* and 5.5% on TreeBench for Qwen2.5-VL-7B. Detailed ablation studies across LVLM architectures and scales further validate the generalizability of our method.

2. Related Work

2.1. Large Vision-Language Models

Early breakthroughs in Large Vision-Language Models (LVLMs), such as Flamingo [1] and BLIP-2 [15], integrated visual features into an LLM via cross-attention. In contrast, LLaVA [18] maps features from a frozen vision encoder (*e.g.*, CLIP [25]) into the LLM’s semantic space with a lightweight MLP. This feature-projection paradigm has driven rapid progress, with subsequent work scaling LVLMs and tackling increasingly complex tasks, such as OCR [17, 47, 48], general VQA [10, 19, 53], and latent visual reasoning [11, 49]. A critical frontier is to handle high-resolution input. For instance, LLaVA-NeXT [19] and InternVL1.5 [5] support arbitrary resolutions, while Qwen2-VL [37] and Qwen2.5-VL [3] introduce mRoPE for resolution generality. Despite these advances, current LVLMs lack an explicit mechanism to perceive and localize task-relevant visual evidence, which leads to hallucinations, especially in high-resolution scenes. We address this gap with DeepScan, a training-free framework that couples LVLMs with external experts to achieve visually grounded reasoning, yielding more accurate and interpretable answers.

2.2. Visually Grounded Reasoning

Recent agents with “*think-with-images*” capabilities (*e.g.*, GPT-o3 [23]) perform visually grounded reasoning that localizes and emphasizes the critical visual content during inference through dynamic image manipulation [23, 33, 44]. Building on this, subsequent works employ SFT and reinforcement learning (RL) with visual rewards [9, 32, 35, 36, 50, 52], or curiosity-driven objectives [31] to reproduce this ability in general LVLMs; SEAL [42] further integrates explicit evidence localization and visual memory. However, these approaches are costly and challenging to generalize to different architectures and model scales. To overcome this, a parallel line explores training-free paradigms that leverage external visual experts [2, 13, 45, 51], tree search [30], or self-refinement [46] to enhance LVLMs by “grounding-then-answering.” Despite these advances, most of them rely on a *coarse-to-fine* grounding strategy, which is sensitive to noisy context and semantically similar objects, resulting in inaccurate localization. By contrast, we propose Hierarchical Scanning, a *bottom-up* grounding paradigm that progressively recovers visual evidence from associated local cues via point-based proxies, enabling robust localization of fine-grained visual evidence in complex scenes.

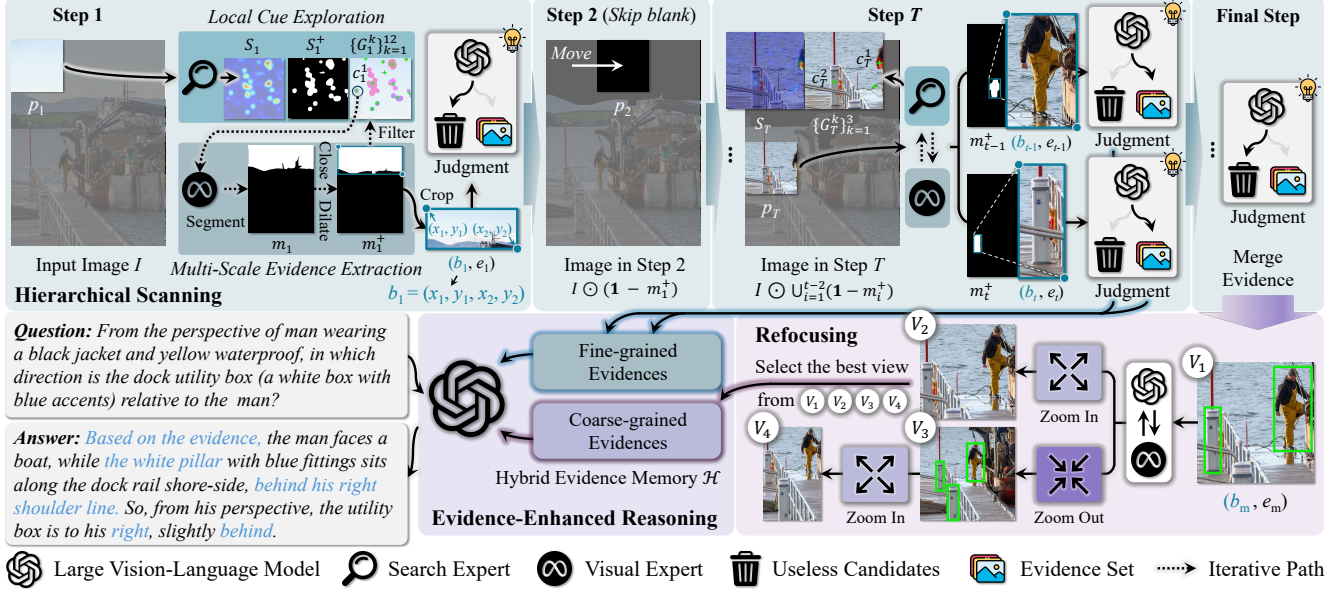


Figure 3. Overall architecture of **DeepScan**: Hierarchical Scanning progressively recovers visual evidence from *in-patch* cues formulated as point-based proxies using Local Cue Exploration and Multi-Scale Evidence Extraction, e.g., $c_T^1 \mapsto e_{t-1}$ in step T ; Refocusing further refines the surrounding context for the fused evidence via interactions between LVLMs and visual experts; Evidence-Enhanced Reasoning leverages a Hybrid Evidence Memory to provide multi-granular information to the LVLm, enabling detailed yet comprehensive answers.

3. Methodology

3.1. Overview

To equip LVLMs with visually grounded reasoning, we propose **DeepScan** that localizes, recalibrates, and integrates visual evidence to produce more accurate and interpretable answers, as shown in Fig. 3. To enhance fine-grained perception, DeepScan augments LVLMs with two *plug-and-play* models, i.e., a search expert and a visual expert. Formally, given an image $I \in \mathbb{R}^{H \times W \times 3}$ with a question q , the search expert highlights the potential cues in a local patch $p \in I$ via its attention map S induced by GradCAM [29]:

$$S = \text{SEARCH}(p, q) \in \mathbb{R}^{h \times w}, \quad p \in \mathbb{R}^{h \times w \times 3}. \quad (1)$$

By contrast, the visual expert exposes two primitives to indicate the image-level evidence: segmentation from a point prompt $c = (x, y) \in I$ and detection from the question q :

$$m = \text{SEGMENT}(I, c), \quad \mathcal{B} = \text{DETECT}(I, q), \quad (2)$$

where m denotes the evidence mask, and \mathcal{B} represents the union of evidence bounding boxes. In this way, the LVLm can generate a well-grounded answer for the question using the image regions enclosed by m or \mathcal{B} . This pipeline is general and training-free, improving LVLMs across architectures and model scales without adaptation cost.

3.2. Hierarchical Scanning

To suppress the effects of irrelevant visual content, a natural idea is to partition the image into patches and perform a

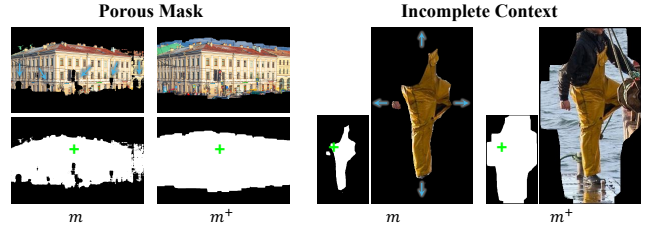


Figure 4. Illustration of morphological post-processing. + marks the point-based proxies; m and m^+ denote evidence masks before and after post-processing, showing improved robustness.

patch-wise evidence extraction. However, this poses a fundamental challenge: when evidence spans multiple patches, conventional proxies (e.g., region proposals [31, 35, 50, 52], detection boxes [13, 24], or textual descriptions [39]) struggle to represent the resulting incomplete evidence.

To address this issue, Hierarchical Scanning introduces novel *point-based proxies* to bridge two well-designed processes, i.e., *patch-wise* Local Cue Exploration and *image-level* Multi-scale Evidence Extraction, thereby enabling a bottom-up visual grounding paradigm.

Local Cue Exploration. Given a patch $p \in \mathbb{R}^{h \times w \times 3}$ from the input image I and a question q , we first apply the search expert and Otsu’s method [?] to produce potential cue regions indicated by a high-value attention mask S_p^+ :

$$S_p^+ = \mathbb{I}(S_p \geq T_p^*) \in \{0, 1\}^{h \times w}, \quad T_p^* = \text{OTSU}(S_p), \quad (3)$$

where $S_p = \text{SEARCH}(p, q) \in \mathbb{R}^{h \times w}$. We then formulate

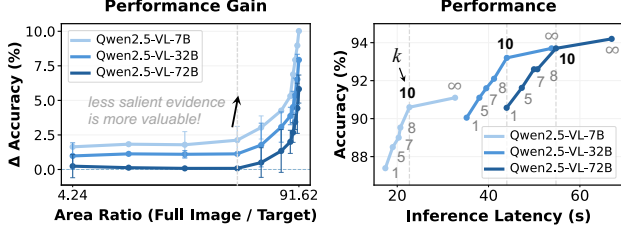


Figure 5. Analysis of (left) performance gain w.r.t. target area ratio and (right) performance-latency trade-off on V^* , where ∞ mark denotes the case *without* explicit truncation of candidate count k .

the cues $\{G_p^k\}_{k=1}^K$ as the connected components in S_p^+ . To associate these cues with evidence, we represent each cue by an interior point derived from its geometric and semantic information, enabling efficient evidence retrieval via point-prompt segmentation. For any interior location $c \in G$, the geometric term is its distance to the cue boundary ∂G :

$$d(c, \partial G) = \inf_{\gamma \in \partial G} \|c - \gamma\|_2. \quad (4)$$

Considering only Eq. (4) can yield multiple candidates for complex cues (e.g., U-shaped regions); we therefore incorporate the attention scores to disambiguate and bias the evidence proxies \mathcal{C}_p toward semantically significant regions:

$$\mathcal{C}_p = \left\{ c_p^k \mid c_p^k = \arg \max_{c \in G_p^k} \tilde{S}_p(c) \tilde{d}(c, \partial G_p^k), |\tilde{d}(c, \partial G_p^k)| \geq \tau \right\}, \quad (5)$$

where τ is a threshold that filters out spurious small cues. $\tilde{S}_p(c)$ is the normalized attention score at c , and $\tilde{d}(c, \partial G_p^k)$ is the normalized distance-to-boundary at c . Finally, we lift these *in-patch* proxies \mathcal{C}_p to the image coordinates for \mathcal{C}_p' .

Multi-scale Evidence Extraction. Given a proxy $c_p' \in \mathcal{C}_p'$ obtained from image I , we employ the visual expert to recover the evidence mask m by point-prompt segmentation:

$$m = \text{SEGMENT}(I, c_p') \in \{0, 1\}^{H \times W}, \quad I \in \mathbb{R}^{H \times W \times 3}. \quad (6)$$

In particular, although the mask m captures image-level evidence, the single-point prompt has limited expressiveness; as a result, m often contains artifacts, e.g., interior holes or incomplete surrounding context, as shown in Fig. 4. To ensure the evidence integrity, we adopt morphological post-processing and produce the enhanced mask m^+ :

$$m^+ = (m \bullet \mathcal{K}) \oplus \mathcal{S}_r, \quad m^+ \in \{0, 1\}^{H \times W}, \quad (7)$$

where \bullet denotes *closing* with a flat kernel \mathcal{K} to seal interior holes, and \oplus denotes *dilation* with a disk kernel \mathcal{S}_r to extend the mask outward. To avoid repeated extraction, we filter any proxies that fall inside the same evidence mask:

$$\mathcal{C}_p' \leftarrow \{c \in \mathcal{C}_p' \mid m^+(c) = 0\}, \quad (8)$$

where $m^+(c)$ denotes the value of m^+ at the location indicated by proxy c . The evidence candidate e is then cropped from the minimal enclosing region b of m^+ . Motivated by [13, 39, 46], we query the LVLM to make a binary judg-

Q: What is the pose of the **woman** with yellow **backpack**?

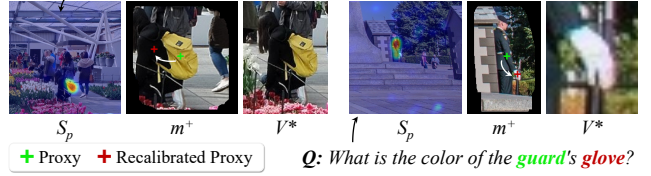


Figure 6. Illustration of Refocusing, where V^* denotes its results. It reveals that Refocusing recalibrates the proxy misalignment by adaptively completing (left) or further amplifying (right) evidence.

ment of the evidence e (detailed in Supp. B) and, if affirmed, update the evidence set $\mathcal{E} \leftarrow \mathcal{E} \cup \{(b, e)\}$.

Finally, we maintain a global visited mask over the examined evidence, i.e., $I \leftarrow I \odot (1 - m^+)$, and bypass the masked region to reduce redundant computation.

Heuristic Acceleration. As shown in Fig. 5(left), localizing less salient evidence leads to a significantly higher performance gain for LVLMS. This is because large evidence regions are often detected by the LVLM without explicit grounding. Therefore, we pre-filter candidates by area and evaluate only the top- k smallest regions, which limits the number of LVLM evaluations to k and reduces the visual-token cost. Empirically, even $k = 1$ preserves about 96% of the maximum achievable performance while yielding roughly a $2\times$ speedup, as presented in Fig. 5(right).

3.3. Refocusing

While Hierarchical Scanning effectively recovers evidence via point-based proxies, precise proxy placement becomes challenging when multiple visual elements are spatially adjacent, often yielding insufficient or excessive surrounding context, as shown in Fig. 6. To address this, we introduce Refocusing, a collaborative search paradigm that integrates the LVLM with the visual expert to identify an evidence-centric view with an optimal surrounding context window.

Initialization. Given an evidence set \mathcal{E} collected by Hierarchical Scanning in image I , we initialize the search with the aggregated evidence, i.e., $V_1 = \text{CROP}(I, b_m)$, where b_m is the minimum bounding box enclosing all evidence.

States & Successor Function. Search states are defined as neighborhoods of V_1 obtained by varying the surrounding context. We design two actions to generate candidate states:

◇ **Zoom-In.** Narrow the surrounding context by cropping V to the union of detections conditioned on query q :

$$\text{IN}(V, q) = \text{CROP}(V, \text{DETECT}(V, q)). \quad (9)$$

◇ **Zoom-Out.** Enlarge the surrounding context by isotropically expanding V with scale $s > 1$ w.r.t. its center:

$$\text{OUT}(V, s) = \text{CROP}(I, \text{SCALEBOX}(V, s)). \quad (10)$$

Selection Policy. Motivated by Fig. 5(left), we prefer the smallest view that still contains all evidence required to an-

swer the question. Accordingly, we define an LVLM-based reward and select the state with the highest score:

$$R(V) = \mathbb{I}_{V \rightsquigarrow q} \cdot HW/hw, \quad V \in \mathbb{R}^{h \times w \times 3}. \quad (11)$$

Here, $\mathbb{I}_{V \rightsquigarrow q}$ is an indicator equal to 1 if V contains sufficient evidence for answering q , and 0 otherwise. In practice, $\mathbb{I}_{V \rightsquigarrow q}$ is obtained from a one-shot binary judgment by the LVLM over the objects in \mathcal{E} (details in Supp. B).

Search Space Design. Unlike existing methods [13, 30] that search the entire image, Hierarchical Scanning provides a well-initialized view V_1 for Refocusing, which motivates the following design principles to prune the search space:

- ◇ The optimal evidence view lies in a neighborhood of V_1 ; thus, *Zoom-In* at V_1 is empirically idempotent:

$$\text{IN}(\text{IN}(V_1, q), q) = \text{IN}(V_1, q) = \textit{evidence}. \quad (12)$$

- ◇ V_1 covers a small fraction of I ; thus, *Zoom-Out* expands V_1 without boundary clipping. Hence, for any $s_1, s_2 \geq 1$,

$$\text{OUT}(\text{OUT}(V_1, s_1), s_2) = \text{OUT}(V_1, s_1 s_2). \quad (13)$$

- ◇ If V_1 already contains complete evidence, *i.e.*, $\mathbb{I}_{V_1 \rightsquigarrow q} = 1$, then $\mathbb{I}_{\text{IN}(V_1, q) \rightsquigarrow q} = \mathbb{I}_{\text{OUT}(\text{IN}(V_1, q), s) \rightsquigarrow q} = 1$, and thus

$$R(\text{OUT}(\text{IN}(V_1, q), s)) \leq R(\text{IN}(V_1, q)). \quad (14)$$

Otherwise (*i.e.*, $\mathbb{I}_{\text{IN}(V_1, q) \rightsquigarrow q} = \mathbb{I}_{V_1 \rightsquigarrow q} = 0$): if *Zoom-Out* fails to restore the missing context for $\text{IN}(V_1, q)$, then

$$R(\text{OUT}(\text{IN}(V_1, q), s)) = 0; \quad (15)$$

if *Zoom-Out* can restore the context for $\text{IN}(V_1, q)$, then it can also restore the context directly from V_1 , and thus

$$R(\text{OUT}(\text{IN}(V_1, q), s)) \leq R(\text{IN}(\text{OUT}(V_1, s), q)). \quad (16)$$

Thus, the state $\text{OUT}(\text{IN}(V_1, q), s)$ can be omitted from the search space without affecting global optimality.

Based on these principles, we construct the search space via only a depth-2 expansion of V_1 and consider a *concise yet behaviorally complete* view set $\mathcal{V} = \{V_1, V_2, V_3, V_4\}$:

$$V_2 = \text{IN}(V_1, q), \quad V_3 = \text{OUT}(V_1, s), \quad V_4 = \text{IN}(V_3, q), \quad (17)$$

where the scale s is set to 1.5 via a grid search. We traverse \mathcal{V} in depth-first order and greedily select the best view.

3.4. Evidence-Enhanced Reasoning

During the preceding stages, we build a hybrid evidence memory \mathcal{H} that stores fine-grained evidence from Hierarchical Scanning and coarse-grained views from Refocusing:

$$\mathcal{H} = \{e, V^* \mid (b, e) \in \mathcal{E}, V^* = \arg \max_{V \in \mathcal{V}} R(V)\}. \quad (18)$$

This hybrid memory \mathcal{H} is then materialized as an ordered *multi-image prompt* $[e_1, \dots, V^*]$. Leveraging this, LVLMs can resolve object attributes from fine-grained evidence and infer relations from coarse-grained views, yielding more comprehensive and accurate answers $\mathcal{A} = \text{REASON}(\mathcal{H}, q)$.

Table 1. Comparisons on V* Bench and HR-Bench, where all the baselines are developed from Qwen2.5-VL-7B, and the RL-based methods are marked by gray. Results[†] are self-collected.

	V* [42]			HR-4K [39]			HR-8K [39]		
	Avg	Att	Spa	Avg	Sin	Cro	Avg	Sin	Cro
General Large Vision-Language Models									
GPT-4o-1120 [22]	66.0	–	–	59.0	70.0	48.0	55.5	62.0	49.0
LLaVA-OV-7B[10]	70.7	73.0	60.5	64.3	74.8	53.8	59.8	65.3	54.3
LLaVA-OV-72B	73.8	80.9	63.2	66.3	76.5	56.0	60.9	68.8	53.0
InternVL3-8B[53]	72.3	73.0	71.1	70.8	79.3	62.3	62.0	64.3	59.8
InternVL3-38B	77.5	77.4	77.6	76.3	83.5	69.0	67.0	71.3	62.8
InternVL3-78B	76.4	75.7	77.6	75.5	84.5	66.5	67.3	71.8	62.8
Qwen2.5VL-7B[3]	74.3	77.4	69.7	72.1	88.8	55.5	68.8	83.5	54.0
Qwen2.5VL-32B	85.9	83.5	89.5	74.8	89.3	60.3	71.6	86.5	56.8
Qwen2.5VL-72B	84.8	90.8	80.9	79.4	88.8	70.0	76.3	84.3	68.3
Visually Grounded Reasoning Models									
PixelReasoner[31]	80.6	83.5	76.3	72.9	86.0	60.3	66.9	80.0	54.3
DeepEyes[52]	90.0	92.1	86.8	75.1	91.3	59.0	72.6	86.8	58.5
Thyme-VL[50]	82.2	83.5	80.3	77.0	91.0	63.0	72.0	86.5	57.5
TreeVGR [†] [35]	85.9	86.1	85.5	72.7	89.5	61.5	69.8	84.4	57.2
ZoomRefine [†] [46]	82.2	85.3	77.6	71.5	88.5	55.3	68.6	83.9	54.0
Dyfo [†] [13]	84.3	82.6	86.8	71.3	89.2	53.5	69.8	86.5	53.2
DeepScan	90.6	93.0	86.8	75.0	90.1	59.7	72.4	87.2	57.6
vs. Qwen2.5-VL-7B	↑16	↑16	↑17	↑2.8	↑1.3	↑4.2	↑3.6	↑3.7	↑3.6

4. Experiments

4.1. Experimental Settings

Datasets & Evaluation Metrics. **V* Bench** contains 191 images with an average resolution of 2246×1582 and emphasizes very small targets (mean area $< 0.05\%$). It covers two tasks: *Direct Attribute* recognition (*Att*, 115 samples) and *Spatial Relationship* reasoning (*Spa*, 76 samples). We report multiple-choice accuracy. **HR-Bench** is available at two resolutions (8K/4K). Each version contains 200 images, split evenly into *Single-Instance Perception* (*Sin*, 100 samples) and *Cross-Instance Perception* (*Cro*, 100 samples). We evaluate using multiple-choice accuracy with a cyclic-permutation protocol. **TreeBench** [35] is designed to assess “*thinking-with-images*” capabilities via three principles: localization of traceable evidence, perception of subtle targets, and second-order reasoning. It provides 405 images with an average resolution of 2152×1615 and reports both multiple-choice accuracy and localization quality (mIoU).

Baseline Methods. We compare DeepScan with RL-based methods [31, 35, 50, 52], training-free methods [13, 46], private models [7, 8, 22, 23], and open-source general models [3, 10, 53]. Further details are provided in Supp. C.

Implementation Details. We adopt BLIP-ITM base [12, 14] as the search expert and LangSAM [21] as the visual expert. To balance performance and latency, we set $k = 10$ in practice. We evaluate DeepScan with 5 LVLMs: LLaVA-1.5-7B, Qwen2-VL-7B, and Qwen2.5-VL-7B / 32B / 72B. We query the LVLM to classify the question type (detailed in Supp. B) and dynamically set the patch size to 576×576 for single-object and 768×768 for multi-object scenarios. All the hyperparameters are listed in Supp. B. All experiments were performed on $4 \times \text{NVIDIA L20 GPUs}$.

Table 2. Comparison with state-of-the-art alternatives on TreeBench [35]. All the baselines are developed from Qwen2.5-VL-7B, and the RL-based methods are marked by gray. Results[†] are self-collected. **DeepScan** achieves competitive results compared to SOTAs.

	Overall mIoU		Perception					Reasoning					Comparison
			Attributes	Material	Phy. State	Obj. Retr.	OCR	Per. Trans.	Ordering	Con. & Oc.	Spa. Cont.		
General Large Vision-Language Models													
Gemini-2.5-Flash-0520 [7]	45.9	–	48.3	53.9	69.6	68.8	75.0	15.3	19.3	56.1	72.4	43.2	
GPT-4o-1120 [22]	46.9	–	51.7	61.5	65.2	43.8	69.1	18.8	38.6	48.8	72.4	43.2	
Gemini-2.5-Pro-0605 [8]	54.1	–	51.7	61.5	56.5	75.0	83.8	20.0	36.8	65.9	86.2	54.6	
GPT-o3-0416 [23]	54.8	–	69.0	69.2	65.2	68.8	79.4	22.4	38.6	61.0	86.2	50.0	
LLaVA-OneVision-7B [10]	37.3	–	55.2	53.8	56.5	50.0	32.4	21.2	22.8	41.5	72.4	36.4	
LLaVA-OneVision-72B	40.5	–	62.1	53.8	65.2	62.3	36.8	12.9	28.1	53.7	65.5	47.7	
Qwen2.5-VL-7B [3]	37.0	–	55.2	53.8	56.5	62.5	27.9	20.0	35.1	39.0	44.8	43.2	
Qwen2.5-VL-32B	42.5	–	51.7	53.8	69.6	62.5	54.4	16.5	33.3	46.3	62.1	38.6	
Qwen2.5-VL-72B	42.2	–	65.5	69.2	56.5	56.3	48.5	11.8	33.3	51.2	72.4	38.6	
InternVL3-8B [53]	38.8	–	51.7	69.2	56.5	56.3	33.7	21.2	24.6	39.0	72.4	43.2	
InternVL3-38B	42.0	–	51.7	61.5	52.2	68.8	51.5	12.9	33.3	56.1	65.5	38.6	
InternVL3-78B	46.4	–	62.1	61.5	52.2	68.8	52.9	16.5	33.3	61.0	86.2	45.5	
Visually Grounded Reasoning Models													
DeepEyes [52]	37.5	30.0	62.1	53.8	65.2	68.8	51.5	11.8	24.6	36.6	51.7	47.7	
Pixel-Reasoner [31]	39.0	35.7	58.6	61.5	65.2	50.0	48.5	14.1	31.6	39.0	44.8	40.9	
TreeVGR [†] [35]	41.0	31.8	55.2	61.5	65.2	50.0	61.7	15.3	24.6	46.3	44.8	40.9	
ZoomRefine [†] [46]	38.0	–	48.3	61.5	56.5	62.5	39.7	18.8	29.8	46.3	44.8	38.6	
Dyfo [†] [13]	39.3	–	58.6	69.2	56.5	62.5	35.3	21.2	35.1	41.5	44.8	40.9	
DeepScan	42.5	37.3	62.1	69.2	60.9	68.8	44.1	21.2	36.8	43.9	48.3	43.2	
Δ vs. Qwen2.5-VL-7B	↑5.5	–	↑6.9	↑15.4	↑4.4	↑6.3	↑16.2	↑1.2	↑1.7	↑4.9	↑3.5	±0.0	

4.2. Main Results

Fine-grained Visual Understanding. As shown in Tab. 1, DeepScan delivers substantial gains over vanilla Qwen2.5-VL-7B across all benchmarks, e.g., 16.3% overall improvement on V*. Compared with the popular general LVLMs, DeepScan attains state-of-the-art performance. Noticeably, it even surpasses several 70B general models on perception tasks, such as the *Attribute* subset in V* Bench and the *Single* subset of HR-Bench, where evidence localization is crucial. Moreover, DeepScan consistently outperforms *all the* training-free baselines, achieving 6.3%, 3.6%, and 2.6% overall gains over DyFo on V* Bench and HR-Bench-4K/8K. Benefiting from the well-designed grounding pipeline, DeepScan remains competitive with leading RL-based methods, e.g., DeepEyes, *without additional fine-tuning* of the LVLm, especially on perception tasks.

General Visual Tasks. In general, RL-based and training-free methods are comparable, as reported in Tab. 2. Specifically, RL-based approaches have clear advantages on complex perception tasks (e.g., Physical State, OCR, etc.), whereas on second-order reasoning tasks (e.g., Perspective Transform, Ordering, etc.) they deliver trivial gains. We hypothesize that RL does not fundamentally strengthen LVLms in visual reasoning; rather, it biases LVLms toward perception behaviors. Furthermore, DeepScan shows strong perception ability, exceeding the RL-based DeepEyes, Pixel-Reasoner, and TreeVGR by 7.3, 1.6, and 5.5 mIoU, respectively, revealing the superiority of Hierarchical Scanning. Based on this, DeepScan attains the best overall results among not only training-free but also RL-based baselines, outperforming DeepEyes, Pixel-Reasoner, and

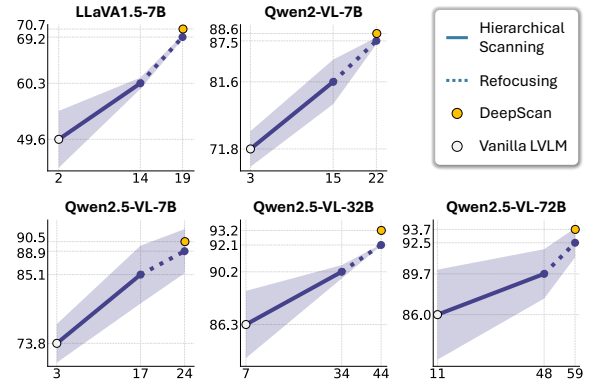


Figure 7. Ablations of DeepScan across LVLms on V*, where the y -axis shows average performance (%), the x -axis reports latency (s), and the shadow shows performance deviation across subsets.

TreeVGR by 5.0%, 3.5%, and 1.5% without fine-tuning.

4.3. Ablation Study

Framework. We conduct ablations of the DeepScan framework in two aspects: its components and overall pipelines. \diamond *Components.* As presented in Fig. 7, DeepScan consistently improves diverse LVLms across architectures and parameter scales without adaptation cost, demonstrating its strong generalization. Besides, Tab. 3 shows that the experts of different sizes deliver similar performance and exhibit comparable memory footprint and latency, indicating that DeepScan is insensitive to the expert scale.

\diamond *Pipelines.* As illustrated in Fig. 7, all stages contribute to the improvement. Specifically, Hierarchical Scanning is the primary driver; Refocusing adds further gains while main-

Table 3. Ablation of external experts on V*; Mem denotes the memory footprint of each DeepScan variant in gigabytes (G). Time reports the average per-sample inference latency in seconds (s).

		Overall	Attribute	Spatial	Mem (\downarrow)	Time (\downarrow)
BLIP-ITM	base	90.6	93.0	86.8	29.4G	24.5s
	large	90.1	92.2	86.8	32.8G	25.8s
LangSAM	small	89.5	93.0	84.2	31.5G	23.2s
	base ⁺	89.5	91.3	86.8	31.9G	24.0s
	large	90.6	93.0	86.8	32.8G	24.5s

Table 4. Ablation of Hierarchical Scanning on V*.

	Overall	Attribute	Spatial	Time (\downarrow)
Detection [13]	82.2	81.7	82.9	13.0s
Hierarchical Scanning	90.6	93.0	86.8	24.5s
w/o Post-Processing	87.4	89.6	85.5	32.1s

Table 5. Ablation of the Local Cue Exploration on V*. *left*: proxy type, where S and T denote semantic and topological information. *right*: patch size, where S / M denotes single-/multi-object scenes.

Proxy	S		T		Att		Spa		S / M			
	✓	✓	✓	✓	✓	✓	✓	✓	Avg	Att	Spa	
Centroid			✓		84.3	80.3			384	87.4	90.4	82.9
Chebyshev Center			✓		91.3	82.9			576	90.1	94.0	84.2
Attention Peak			✓		87.8	85.5			768	88.5	88.7	88.2
Ours	✓	✓	✓	✓	93.0	86.8			576 / 768	90.6	93.0	86.8

taining a favorable performance–latency trade-off. Building on them, Evidence-Enhanced Reasoning delivers additional improvements with negligible overhead. This demonstrates the completeness of the DeepScan framework.

Hierarchical Scanning As shown in Tab. 4, compared with the detection-based grounding method applied in Dyfo [13], Hierarchical Scanning delivers obvious overall gains, with particularly large improvements on the *Attribute* subset.

◇ *Morphological Post-Processing*. As shown in Tab. 4, it fills interior holes in evidence masks; thus, it not only yields clear performance gains but markedly accelerates inference by preventing repeated processing of the same evidence.

◇ *Evidence Proxy*. As shown in Tab. 5(*left*), centroid-based proxies can fall outside U-shaped cues, which compromises evidence recovery and degrades the overall performance. In contrast, attention peak and Chebyshev center provide complementary performance gains across scenes, while our design Eq. (5) fuses them and yields noticeably better results.

◇ *Patch Size*. As reported in Tab. 5(*right*), smaller patches are more effective at suppressing context and yield better performance in single-object scenes, while larger patches are preferred in multi-object scenes because context provides valuable spatial relations. Accordingly, we condition patch size on the scene type to enhance overall performance.

Refocusing. We conduct ablations of refocusing in three aspects: action set, search-space design, and zoom-out scale.

◇ *Action Set*. Tab. 6(*left*) shows that both actions are indispensable: removing either action degrades performance, whereas using them jointly yields consistent gains.

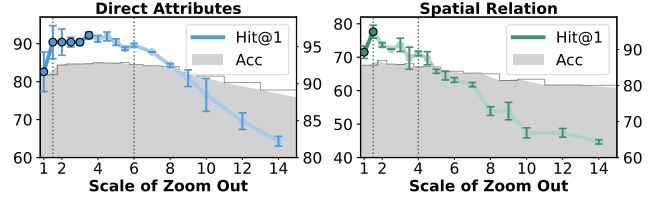


Figure 8. Ablation of the *Zoom-Out* scale on V*, where the left y-axis shows Hit@1 of evidence detection on the zoomed-out view, while the right y-axis shows the accuracy (Acc) of DeepScan.

Table 6. *Left*: effects of each action; *Right*: comparison of search length with different search methods and search space design.

IN		OUT		Att		Spa				
✓				89.6	73.7	MCTS	7	2.24	4	
	✓			87.8	72.4	A*	7	3.07	4	
✓	✓			93.0	86.8	Ours	4	1.87	4	

◇ *Search Space Design*. We evaluate both search efficiency and search space completeness using *search length*, defined as the mean number of expansions required to first reach the oracle-optimal state. In ablation, MCTS and A* enumerate all depth-2 reachable states and score each using Eq. (11), whereas *Refocusing* visits only the states in \mathcal{V} . As shown in Tab. 6(*right*), under the same expansion budget, *Refocusing* exhibits a shorter search length, empirically supporting our design principles and indicating both the completeness of the search space and the efficiency of the selection policy.

◇ *Scale of Zoom-Out*. Fig. 8 shows that a moderate *Zoom-Out* recalibrates evidence, *i.e.*, higher Hit@1, and increases DeepScan accuracy, while overly large *Zoom-Outs* bring excessive context and impair both grounding and reasoning. DeepScan shows greater tolerance to *Zoom-Out* in *Direct Attributes*, which is attributed to their smaller initial views.

4.4. In-depth Analysis

Case Study. Fig. 9 presents case studies from V* Bench and TreeBench. Specifically, GPT-4o and DyFo easily suffer from attention drift, leading to mislocalization and incorrect answers; in contrast, DeepScan accurately localizes evidence and produces interpretable answers (Fig. 9a, c). Furthermore, DeepScan precisely grounds ultra-subtle evidence (area ratio $<1\%$) and generates correct answers, demonstrating the effectiveness of Hierarchical Scanning (Fig. 9b, d). TreeBench typically involves long queries and complex visual reasoning. Despite this, DeepScan consistently identifies evidence and enhances LVLMs via visually grounded reasoning, revealing its robustness (Fig. 9c, d).

Analysis of Grounding Paradigms. The key insight of DeepScan is the *bottom-up* grounding paradigm. To further reveal its fundamental superiority, we design a *one-shot* variant of Hierarchical Scanning that performs *image-level* rather than *patch-wise* cue exploration, and provide qualitative and quantitative comparisons between the two variants.

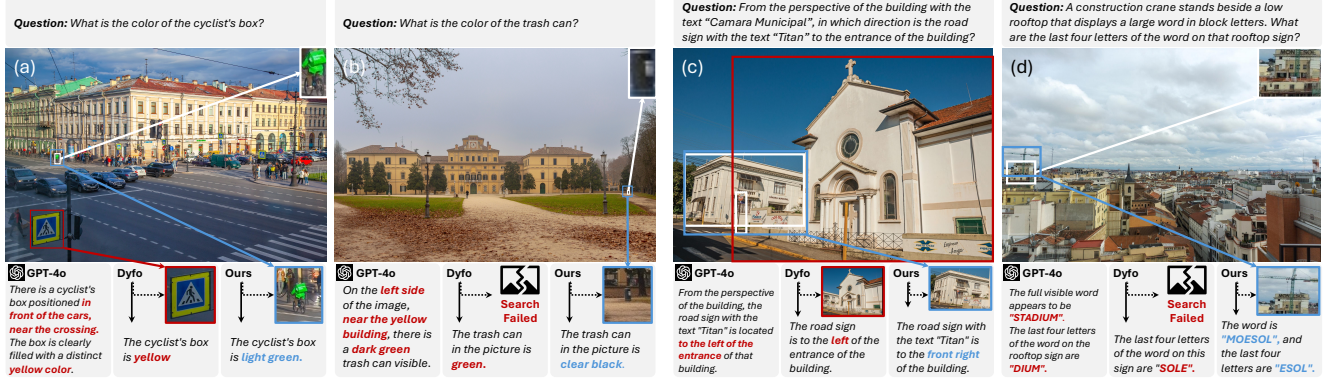


Figure 9. Case study of grounding results and model responses of GPT-4o, DyFo, and the proposed DeepScan. Panels (a–b) are from V* Bench; panels (c–d) are from TreeBench. Correct and incorrect responses are highlighted in blue and red text, respectively. GT, evidence searched by DyFo, and evidence localized by DeepScan are marked in the image using white, red, and blue bboxes, respectively.

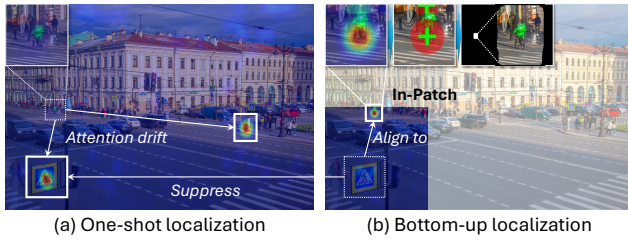


Figure 10. Qualitative analysis of the grounding paradigms with the attention map S of the search expert in Fig. 9 (a).

Table 7. Quantitative analysis of the grounding paradigms on V*.

	Overall	Attribute	Spatial	Time (\downarrow)
One-shot Localization	83.8	83.5	84.2	20.4s
Bottom-up Localization	90.6	93.0	86.8	24.5s

◇ *Qualitative Analysis.* As shown in Fig. 10, the one-shot variant exhibits errors similar to DyFo with distinct experts (GroundingDINO vs. BLIP), where attention drifts toward the same object, “box sign.” This highlights the general impact of attention sink/drift on visual grounding. By contrast, the bottom-up variant suppresses the distractions and aligns attention with the correct target “cyclist’s box”, revealing the fundamental advantage of the bottom-up paradigm.

◇ *Quantitative Analysis.* As reported in Tab. 7, bottom-up localization clearly outperforms one-shot localization, particularly on fine-grained tasks. Moreover, the one-shot variant does not achieve a markedly higher inference speed than the bottom-up one. We attribute this to the proxy filtering in the evidence extraction, which keeps the LVLM judgment counts roughly comparable between the two paradigms.

Impact of Grounding on LVLM Reasoning. We study the reasoning performance in Qwen2.5-VL series under varying grounding precision, achieved by cropping the target with different sizes of surrounding context from the images on V*. As shown in Fig. 11, we point out two key insights:

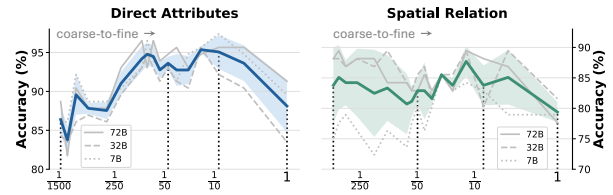


Figure 11. Performance of Qwen2.5-VL series with the varying grounding precision (measured by IoU) on V* Bench.

- ◇ *More aggressive grounding is not always better.* Excessive zoom-in, e.g., IoU from 1/10 to 1, can remove essential context and thus degrade LVLM reasoning. Consistent with this observation, our selection policy avoids naively favoring smaller crops: the state reward Eq. (11) pairs a size regularizer with LVLM feedback to discourage over-cropping.
- ◇ *Scaling effect benefits second-order reasoning more significantly than perception.* Under precise grounding, perception performance converges across model scales, while spatial reasoning gaps remain. This observation suggests using a lightweight LVLM for evidence judgment, and reserving a large-scale LVLM for Evidence-Enhanced Reasoning, preserving performance yet reducing latency.

5. Conclusion

We present DeepScan, a training-free framework for visually grounded reasoning in LVLMs via explicit evidence localization, recalibration, and integration before answering. Leveraging bottom-up Hierarchical Scanning, DeepScan mitigates effects of noisy context and precisely localizes critical visual content. It further refines the evidence view via Refocusing, yielding more accurate and grounded answers. Experiments show that DeepScan delivers superior performance across diverse visual tasks and substantially improves various LVLMs spanning architectures and parameter scales. Comprehensive ablations and analyses provide additional insights for the LVLM community.

Acknowledgments

This work was supported by the National Natural Science Foundation of China (62176091) and the Natural Science Foundation of Chongqing (CSTB2024NSCQ-MSX0877).

References

- [1] Jean-Baptiste Alayrac, Jeff Donahue, Pauline Luc, Antoine Miech, Iain Barr, Yana Hasson, Karel Lenc, Arthur Mensch, Katherine Millican, Malcolm Reynolds, et al. Flamingo: a visual language model for few-shot learning. *NeurIPS*, 35: 23716–23736, 2022. 2
- [2] Wenbin An, Feng Tian, Sicong Leng, Jiahao Nie, Haonan Lin, QianYing Wang, Ping Chen, Xiaoqin Zhang, and Shijian Lu. Mitigating object hallucinations in large vision-language models with assembly of global and local attention. In *CVPR*, pages 29915–29926, 2025. 1, 2
- [3] Shuai Bai, Keqin Chen, Xuejing Liu, Jialin Wang, Wenbin Ge, Sibo Song, Kai Dang, Peng Wang, Shijie Wang, Jun Tang, et al. Qwen2.5-vl technical report. *arXiv preprint arXiv:2502.13923*, 2025. 2, 5, 6
- [4] Keqin Chen, Zhao Zhang, Weili Zeng, Richong Zhang, Feng Zhu, and Rui Zhao. Shikra: Unleashing multimodal LLM’s referential dialogue magic. *arXiv preprint arXiv:2306.15195*, 2023. 1
- [5] Zhe Chen, Weiyun Wang, Hao Tian, Shenglong Ye, Zhangwei Gao, Erfei Cui, Wenwen Tong, Kongzhi Hu, Jiapeng Luo, Zheng Ma, et al. How far are we to gpt-4v? closing the gap to commercial multimodal models with open-source suites. *Sci. China Inf. Sci.*, 67(12):220101, 2024. 2
- [6] Zhanzhan Cheng, Fan Bai, Yunlu Xu, Gang Zheng, Shiliang Pu, and Shuigeng Zhou. Focusing attention: Towards accurate text recognition in natural images. In *ICCV*, pages 5076–5084, 2017. 2
- [7] DeepMind. Gemini-2.5-flash. <https://deepmind.google/models/gemini/flash/>, 2025. 5, 6
- [8] DeepMind. Gemini-2.5-pro. <https://deepmind.google/models/gemini/pro/>, 2025. 5, 6
- [9] Xin Lai, Junyi Li, Wei Li, Tao Liu, Tianjian Li, and Hengshuang Zhao. Mini-o3: Scaling up reasoning patterns and interaction turns for visual search. *arXiv preprint arXiv:2509.07969*, 2025. 2
- [10] Bo Li, Yuanhan Zhang, Dong Guo, Renrui Zhang, Feng Li, Hao Zhang, Kaichen Zhang, Peiyuan Zhang, Yanwei Li, Ziwei Liu, et al. Llava-onevision: Easy visual task transfer. *arXiv preprint arXiv:2408.03326*, 2024. 2, 5, 6
- [11] Chengzu Li, Wenshan Wu, Huanyu Zhang, Yan Xia, Shaoguang Mao, Li Dong, Ivan Vulić, and Furu Wei. Imagine while reasoning in space: Multimodal visualization-of-thought. In *The Forty-Second International Conference on Machine Learning*, 2025. 2
- [12] Dongxu Li, Junnan Li, Hung Le, Guangsen Wang, Silvio Savarese, and Steven C.H. Hoi. LAVIS: A one-stop library for language-vision intelligence. In *ACL*, pages 31–41, Toronto, Canada, 2023. 5
- [13] Geng Li, Jinglin Xu, Yunzhen Zhao, and Yuxin Peng. Dyfo: A training-free dynamic focus visual search for enhancing Imms in fine-grained visual understanding. In *CVPR*, pages 9098–9108, 2025. 1, 2, 3, 4, 5, 6, 7
- [14] Junnan Li, Dongxu Li, Caiming Xiong, and Steven Hoi. Blip: Bootstrapping language-image pre-training for unified vision-language understanding and generation. In *ICML*, pages 12888–12900. PMLR, 2022. 5
- [15] Junnan Li, Dongxu Li, Silvio Savarese, and Steven Hoi. Blip-2: Bootstrapping language-image pre-training with frozen image encoders and large language models. In *ICML*, pages 19730–19742, 2023. 2
- [16] Yangfu Li, Hongjian Zhan, Tianyi Chen, Qi Liu, Yu-Jie Xiong, and Yue Lu. Why $1 + 1 < 1$ in visual token pruning: Beyond naive integration via multi-objective balanced covering. In *NeurIPS*, 2025. 1
- [17] Yangfu Li, Hongjian Zhan, Qi Liu, Li Sun, Yu-Jie Xiong, and Yue Lu. Msa2: Multi-task framework with structure-aware and style-adaptive character representation for open-set chinese text recognition. In *ICCV*, pages 23095–23104, 2025. 2
- [18] Haotian Liu, Chunyuan Li, Qingyang Wu, and Yong Jae Lee. Visual instruction tuning. *NeurIPS*, 36:34892–34916, 2023. 2
- [19] Haotian Liu, Chunyuan Li, Yuheng Li, Bo Li, Yuanhan Zhang, Sheng Shen, and Yong Jae Lee. Llava-next: Improved reasoning, ocr, and world knowledge. <https://llava-vl.github.io/blog/2024-01-30-llava-next/>, 2024. 2
- [20] Shilong Liu, Zhaoyang Zeng, Tianhe Ren, Feng Li, Hao Zhang, Jie Yang, Qing Jiang, Chunyuan Li, Jianwei Yang, Hang Su, et al. Grounding dino: Marrying dino with grounded pre-training for open-set object detection. In *ECCV*, pages 38–55. Springer, 2024. 1
- [21] Luca Medeiros. Language segment-anything: Sam with text prompt. <https://github.com/luca-medeiros/lang-segment-anything>, 2024. 1, 5
- [22] OpenAI. Openai-gpt-4o. <https://openai.com/index/gpt-4o-system-card/>, 2024. 5, 6
- [23] OpenAI. Openai-o3. <https://openai.com/index/introducing-o3-and-o4-mini/>, 2025. 2, 5, 6
- [24] Jiaxu Qian, Chendong Wang, Yifan Yang, Chaoyun Zhang, Huiqiang Jiang, Xufang Luo, Yu Kang, Qingwei Lin, Anlan Zhang, Shiqi Jiang, et al. Zoomer: Adaptive image focus optimization for black-box mllm. *arXiv preprint arXiv:2505.00742*, 2025. 1, 3
- [25] Alec Radford, Jong Wook Kim, Chris Hallacy, Aditya Ramesh, Gabriel Goh, Sandhini Agarwal, Girish Sastry, Amanda Askell, Pamela Mishkin, Jack Clark, et al. Learning transferable visual models from natural language supervision. In *ICML*, pages 8748–8763, 2021. 2
- [26] Hanoona Rasheed, Muhammad Maaz, Sahal Shaji, Abdelrahman Shaker, Salman Khan, Hisham Cholakkal, Rao M. Anwer, Eric Xing, Ming-Hsuan Yang, and Fahad Shahbaz Khan. GLaMM: Pixel grounding large multimodal model. In *CVPR*, pages 13009–13018, 2024. 1
- [27] Tianhe Ren, Qing Jiang, Shilong Liu, Zhaoyang Zeng, Wenlong Liu, Han Gao, Hongjie Huang, Zhengyu Ma, Xiaoke Jiang, Yihao Chen, et al. Grounding dino 1.5: Advance

- the “edge” of open-set object detection. *arXiv preprint arXiv:2405.10300*, 2024. 1
- [28] Gabriel Sarch, Snigdha Saha, Naitik Khandelwal, Ayush Jain, Michael J Tarr, Aviral Kumar, and Katerina Fragkiadaki. Grounded reinforcement learning for visual reasoning. *arXiv preprint arXiv:2505.23678*, 2025. 3
- [29] Ramprasaath R. Selvaraju, Michael Cogswell, Abhishek Das, Ramakrishna Vedantam, Devi Parikh, and Dhruv Batra. Grad-cam: Visual explanations from deep networks via gradient-based localization. In *ICCV*, pages 618–626, 2017. 3
- [30] Haozhan Shen, Kangjia Zhao, Tiancheng Zhao, Ruochen Xu, Zilun Zhang, Mingwei Zhu, and Jianwei Yin. Zoomeye: Enhancing multimodal llms with human-like zooming capabilities through tree-based image exploration. In *EMNLP*, pages 6613–6629, 2025. 2, 5
- [31] Alex Su, Haozhe Wang, Weiming Ren, Fangzhen Lin, and Wenhui Chen. Pixel reasoner: Incentivizing pixel space reasoning via curiosity-driven reinforcement learning. In *NeurIPS*, 2025. 1, 2, 3, 5, 6
- [32] Zhaochen Su, Linjie Li, Mingyang Song, Yunzhuo Hao, Zhengyuan Yang, Jun Zhang, Guanjie Chen, Jiawei Gu, Juntao Li, Xiaoye Qu, et al. Openthinking: Learning to think with images via visual tool reinforcement learning. *arXiv preprint arXiv:2505.08617*, 2025. 2
- [33] Zhaochen Su, Peng Xia, Hangyu Guo, Zhenhua Liu, Yan Ma, Xiaoye Qu, Jiaqi Liu, Yanshu Li, Kaide Zeng, Zhengyuan Yang, et al. Thinking with images for multimodal reasoning: Foundations, methods, and future frontiers. *arXiv preprint arXiv:2506.23918*, 2025. 2
- [34] Feng Wang, Yaodong Yu, Wei Shao, Yuyin Zhou, Alan Yuille, and Cihang Xie. Scaling laws in patchification: An image is worth 50,176 tokens and more. In *ICML*, 2025. 1
- [35] Haochen Wang, Xiangtai Li, Zilong Huang, Anran Wang, Jiachong Wang, Tao Zhang, Sule Bai, Zijian Kang, Jiashi Feng, Wang Zhuochen, et al. Traceable evidence enhanced visual grounded reasoning: Evaluation and method. In *ICLR*, 2026. 1, 2, 3, 5, 6
- [36] Jiacong Wang, Zijian Kang, Haochen Wang, Haiyong Jiang, Jiawen Li, Bohong Wu, Ya Wang, Jiao Ran, Xiao Liang, Chao Feng, et al. Vgr: Visual grounded reasoning. *arXiv preprint arXiv:2506.11991*, 2025. 2
- [37] Peng Wang, Shuai Bai, Sinan Tan, Shijie Wang, Zhihao Fan, Jinze Bai, Keqin Chen, Xuejing Liu, Jialin Wang, Wenbin Ge, et al. Qwen2-vl: Enhancing vision-language model’s perception of the world at any resolution. *arXiv preprint arXiv:2409.12191*, 2024. 2
- [38] Sisi Wang, Stanislas Huynh Cong, and Geoffrey F Woodman. Statistical learning speeds visual search: More efficient selection, or faster response? *J. Exp. Psychol.: Gen.*, 152(6): 1723, 2023. 1
- [39] Wenbin Wang, Liang Ding, Minyan Zeng, Xiabin Zhou, Li Shen, Yong Luo, Wei Yu, and Dacheng Tao. Divide, conquer and combine: A training-free framework for high-resolution image perception in multimodal large language models. In *AAAI*, pages 7907–7915, 2025. 1, 3, 4, 5
- [40] Jeremy M Wolfe. Visual search: How do we find what we are looking for? *Annu. Rev. Vis. Sci.*, 6(1):539–562, 2020. 1
- [41] Jeremy M Wolfe and Todd S Horowitz. Five factors that guide attention in visual search. *Nat. Hum. Behav.*, 1(3): 0058, 2017. 1
- [42] Penghao Wu and Saining Xie. V*: Guided visual search as a core mechanism in multimodal llms. In *CVPR*, pages 13084–13094, 2024. 1, 2, 5, 3
- [43] Guangxuan Xiao, Yuandong Tian, Beidi Chen, Song Han, and Mike Lewis. Efficient streaming language models with attention sinks. In *ICLR*, 2024. 2
- [44] Junlin Xie, Zhihong Chen, Ruifei Zhang, Xiang Wan, and Guanbin Li. Large multimodal agents: A survey. *arXiv preprint arXiv:2402.15116*, 2024. 2
- [45] Haoxuan You, Haotian Zhang, Zhe Gan, Xianzhi Du, Bowen Zhang, Zirui Wang, Liangliang Cao, Shih-Fu Chang, and Yinfei Yang. Ferret: Refer and ground anything anywhere at any granularity. In *ICLR*, 2024. Spotlight. 1, 2
- [46] Xuan Yu, Dayan Guan, Michael Ying Yang, and Yanfeng Gu. Zoom-refine: Boosting high-resolution multimodal understanding via localized zoom and self-refinement. *arXiv preprint arXiv:2506.01663*, 2025. 1, 2, 4, 5, 6, 3
- [47] Hongjian Zhan, Yangfu Li, Yu-jie Xiong, and Yue Lu. Fare: A feature-aware radical encoding strategy for zero-shot chinese character recognition. In *Proceedings of the Asian Conference on Computer Vision*, pages 390–401, 2024. 2
- [48] Hongjian Zhan, Yangfu Li, Yu-Jie Xiong, Umapada Pal, and Yue Lu. Free lunch: Frame-level contrastive learning with text perceiver for robust scene text recognition in lightweight models. In *ACM MM*, pages 6202–6211, 2024. 2
- [49] Huanyu Zhang, Wenshan Wu, Chengzu Li, Ning Shang, Yan Xia, Yangyu Huang, Yifan Zhang, Li Dong, Zhang Zhang, Liang Wang, et al. Latent sketchpad: Sketching visual thoughts to elicit multimodal reasoning in mllms. *arXiv preprint arXiv:2510.24514*, 2025. 2
- [50] Yi-Fan Zhang, Xingyu Lu, Shukang Yin, Chaoyou Fu, Wei Chen, Xiao Hu, Bin Wen, Kaiyu Jiang, Changyi Liu, Tianke Zhang, et al. Thyme: Think beyond images. *arXiv preprint arXiv:2508.11630*, 2025. 1, 2, 3, 5
- [51] Zheng Zhang, Yeyao Ma, Enming Zhang, and Xiang Bai. Psalm: Pixelwise segmentation with large multi-modal model. In *ECCV*, pages 74–91. Springer, 2024. 1, 2
- [52] Ziwei Zheng, Michael Yang, Jack Hong, Chenxiao Zhao, Guohai Xu, Le Yang, Chao Shen, and Xing Yu. Deep-eyes: Incentivizing “thinking with images” via reinforcement learning. *arXiv preprint arXiv:2505.14362*, 2025. 1, 2, 3, 5, 6
- [53] Jinguo Zhu, Weiyun Wang, Zhe Chen, Zhaoyang Liu, Shenglong Ye, Lixin Gu, Hao Tian, Yuchen Duan, Weijie Su, Jie Shao, et al. Internvl3: Exploring advanced training and test-time recipes for open-source multimodal models. *arXiv preprint arXiv:2504.10479*, 2025. 2, 5, 6

DeepScan: A Training-Free Framework for Visually Grounded Reasoning in Large Vision-Language Models

Supplementary Material

OUTLINE

§ A **Discussions** includes the *failure cases* of DeepScan, limitations and future work, and Broader Impacts, delivering valuable insights.

§ B **Methodological Details** provides pseudocode, the exact prompts applied, and hyperparameter settings.

§ C **Additional Results** conducts a comparison against strong baselines and reveals the state-of-the-art performance achieved by DeepScan on fine-grained tasks.

§ D **Additional Cases** including the advantage of the *bottom-up* grounding paradigm and the Example Model Outputs

A. Discussions

Failure Cases. Based on our analysis, DeepScan’s failures mainly fall into two categories.

(1) *Grounding failure.* In direct-attribute recognition, when multiple visually similar objects remain within the evidence neighborhood, the experts may propose incorrect evidence and the LVLMM may misjudge it, leading to an incorrect evidence localization; and thus the LVLMM produces an incorrect answer based on wrong evidence (see Fig. 12).

(2) *Reasoning failure.* For spatial-relation reasoning with multiple pieces of evidence, DeepScan currently forms a merged evidence view via the minimal enclosing bounding box over all localized evidence. When the evidence is widely separated, this large crop introduces substantial inter-evidence noisy context that hampers reasoning; the issue is exacerbated when the merged view includes distracting content that conflicts with the correct answer (see Fig. 13). This points to a promising direction: replace the minimal enclosing box with a generative composition that reassembles localized fine-grained evidence into a compact layout, suppressing inter-evidence context while preserving object attributes and spatial relations.

Limitations. Compared with one-shot evidence-detection pipelines for visually grounded reasoning, DeepScan has higher inference latency. Nevertheless, as a test-time scaling paradigm, DeepScan offers a controllable performance-efficiency trade-off by tuning the patch size and the number of evidence proposals. In practice, its overall performance-efficiency profile remains acceptable relative to advanced visually grounded models (*e.g.*, GPT-5), as detailed in §D (Example Model Outputs). DeepScan’s current implementation sets a relatively small patch size per image to capture fine-grained cues, which is unnecessary and inefficient for

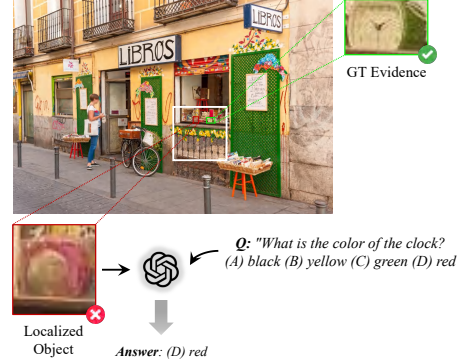


Figure 12. Case study of grounding failure

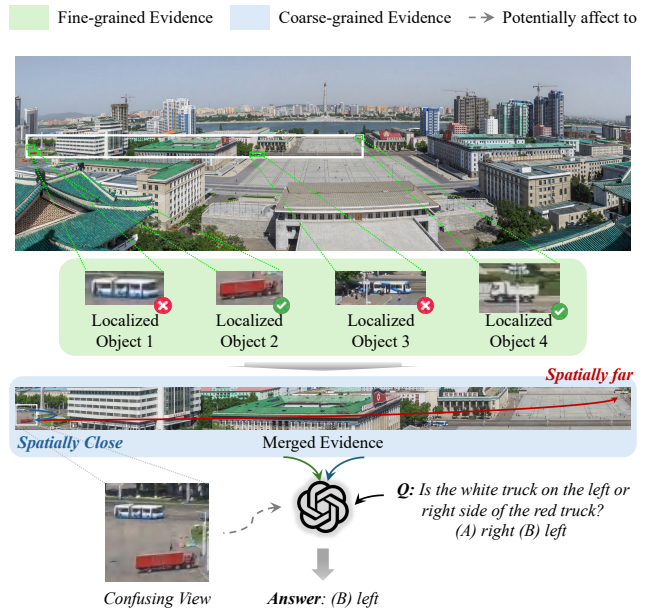


Figure 13. Case study of reasoning failure

simple cases with salient evidence. In the future, we plan to develop an adaptive partition strategy that flexibly assigns a specific patch size within each grounding process based on stronger priors (*e.g.*, evidence saliency), which is expected to further improve the performance-efficiency trade-off.

Broader Impacts. We propose DeepScan, a training-free visually grounded reasoning framework that replaces brittle one-shot localization with hierarchical scanning and refocusing. By tying answers to concrete visual evidence and making contextual extent explicit, DeepScan can benefit domains needing reliable, fine-grained perception under clut-

System Prompt

You are an advanced image understanding assistant. You will be given an image and a question about it.

User Prompt 1 (Evidence Decomposition)

Task: List objects mentioned in text in List format.
Input text: {question}
Action: What objects are mentioned in original text? List separated by commas. For example, from “person with white trousers on the left or right side of the person in blue”, output “[“person with white trousers”, “person in blue”]”.

User Prompt 2 (Evidence Judgment)

I will provide you an image and a ****question****: {question}, please firstly determine whether the image contains the clues for answering the question or not (answer with ****Yes**** or ****No****); then give the evidence of your decision.

User Prompt 3 (View Completeness Justification)

Question: Does the image fully contain every object in the list {target_list}? Please treat “fully contain” as entirely within the frame (not truncated by image boundaries). Please firstly answer the question with ****Yes**** or ****No****; then give the evidence of your decision. For example, if yes, list the evidence of each object (e.g., object: bbox [x1, y1, x2, y2] or a clear region description); if no, list the missing objects by name.

ter and occlusion. Examples include GUI agents (anchoring actions to the correct widget, explaining clicks), embodied manipulation (grasping small parts), and autonomous driving (partially occluded signs). Potential risks include propagation of biases inherited from LVLMs and experts, and automation errors in safety-critical settings. Besides, as a test-time scaling paradigm, DeepScan introduces extra inference overhead, which may limit deployment in compute-constrained scenarios such as edge or mobile devices.

B. Methodological Details

Prompts. We provide below the prompts involved in Sec. 3: (i) *Evidence Decomposition* (to set the patch size), (ii) *Evidence Judgment* in *Hierarchical Scanning*, and (iii) *View*

Algorithm 1 Hierarchical Scanning with Acceleration

Require: image $I \in \mathbb{R}^{H \times W \times 3}$, question q , patch size $\{l_s, l_c\}$, candidate count k , kernel \mathcal{K} , \mathcal{S}_r , threshold $\tau_{\text{area}}, \theta_{\text{IoU}}$

Ensure: Evidence set $\mathcal{E} = \{(b_i, e_i)\}$

- 1: $\mathcal{E}_{\text{all}} \leftarrow \emptyset, \quad \mathcal{E} \leftarrow \emptyset$
- 2: $l \leftarrow \text{SELECTBYLEN}(\text{LVLM}(\text{Prompt1}(q)), \{l_s, l_c\})$
- 3: **for each** patch p in $\text{PARTITION}(I, l)$ **do**
- 4: $S_p \leftarrow \text{SEARCH}(p, q)$
- 5: $S_p^+ \leftarrow \mathbb{I}(S_p \geq \text{OTSU}(S_p))$
- 6: **for each** $G \in \text{CONNCOMP}(S_p^+)$ with $|G| \geq \tau$ **do**
- 7: $d_G(i, j) \leftarrow \inf_{\gamma \in \partial G} \|(i, j) - \gamma\|_2, \forall (i, j) \in G$
- 8: $\tilde{S}_p \leftarrow \text{NORM}(S_p), \quad \tilde{d} \leftarrow \text{NORM}(d_G)$
- 9: $c^* \leftarrow \arg \max_{c \in G} \tilde{S}_p(c) \cdot \tilde{d}(c)$
- 10: $c' \leftarrow \text{LIFTTOIMAGE}(c^*, p \rightarrow I), \quad \mathcal{C}'_p \cup \{c'\}$
- 11: **while** \mathcal{C}'_p not empty **do**
- 12: $c \leftarrow \text{POP}(\mathcal{C}'_p), \quad m \leftarrow \text{SEGMENT}(I, c)$
- 13: $m^+ \leftarrow (m \bullet \mathcal{K}) \oplus \mathcal{S}_r$
- 14: $b \leftarrow \text{BBOX}(m^+), \quad e \leftarrow \text{CROP}(I, b)$
- 15: **if** $\text{IoU}(b, b_i) \leq \theta_{\text{IoU}}$ for all $(b_i, e_i) \in \mathcal{E}_{\text{all}}$ **then**
- 16: $\mathcal{E}_{\text{all}} \leftarrow \mathcal{E}_{\text{all}} \cup \{(b, e)\}$
- 17: $I \leftarrow I \odot (\mathbf{1} - m^+), \quad \mathcal{C}'_p \leftarrow \{c' \in \mathcal{C}'_p \mid m^+(c') = 0\}$
- 18: $\mathcal{E}_k \leftarrow \text{TAKEKSMALLESTBYAREA}(\mathcal{E}_{\text{all}}, k)$
- 19: **for each** $(b, e) \in \mathcal{E}_k$ **do**
- 20: **if** $\text{LVLM}(e, \text{Prompt2}(q)) = \text{Yes}$ **then**
- 21: $\mathcal{E} \leftarrow \mathcal{E} \cup \{(b, e)\}$
- 22: **return** \mathcal{E}

Algorithm 2 Refocusing

Require: image $I \in \mathbb{R}^{H \times W \times 3}$, question q , target list t , evidence set \mathcal{E}

Ensure: refined view V

- 1: $\mathcal{R} \leftarrow \emptyset, \quad b_m \leftarrow \bigcup_{(b, e) \in \mathcal{E}} b$
- 2: $e_m \leftarrow \text{CROP}(I, b_m), \quad V_1 \leftarrow e_m$
- 3: $V_2 \leftarrow \text{IN}(V_1, q), \quad V_3 \leftarrow \text{OUT}(V_1), \quad V_4 \leftarrow \text{IN}(V_3, q)$
- 4: **for** $V \in \{V_1, V_2, V_3, V_4\}$ **do**
- 5: **if** $\text{LVLM}(V, \text{UserPrompt3}(t)) = \text{Yes}$ **then**
- 6: $h, w \leftarrow \text{SHAPE}(V)$
- 7: $R \leftarrow HW/hw$
- 8: **else**
- 9: $R \leftarrow 0$
- 10: $\mathcal{R} \leftarrow \mathcal{R} \cup \{R\}$
- 11: $i^* \leftarrow \arg \max_{i \in \{1, 2, 3, 4\}} \mathcal{R}(i)$
- 12: **return** V_{i^*}

Completeness Justification in Refocusing.

Hyper-Parameters. In *Local Cue Exploration*, the area threshold for noisy-cue filtering is set to 50 pixels. In *Multi-Scale Evidence Extraction*, morphological post-processing uses a 5×5 flat structuring element \mathcal{K} and a disk \mathcal{S}_r with ra-

Table 8. Comparisons between the proposed DeepScan and existing visually grounded reasoning approaches. Like most test-time scaling paradigms, DeepScan is easier to scale up. Furthermore, DeepScan introduces hierarchical scanning and refocusing for a robust bottom-up evidence localization and recalibration and leverages hybrid granular evidence to enable LVLM to produce higher-quality answers.

Methods	Venue	Ease to Scaling	External Experts	Search Strategy	Grounding Paradigm	Evidence Granularity	Inference Latency
Seal [42]	CVPR'24	✗	✗	LLM-guided Search	Coarse-to-Fine	Fine	High
Dyfo [13]	CVPR'25	✓	✓	Detection + MCTS	Coarse-to-Fine	Coarse	High
DeepEyes [52]	NeurIPS'25	✗	✗	Generative Bbox	Coarse-to-Fine	Fine	High
PixelReasoner [31]	NeurIPS'25	✗	✗	Generative Bbox	Coarse-to-Fine	Coarse	High
ViGoRL [28]	NeurIPS'25	✗	✗	Generative Bbox	Coarse-to-Fine	Fine	High
ZoomRefine [46]	NeurIPS'25	✓	✗	Generative Bbox	Coarse-to-Fine	Coarse	Medium
TreeVGR [35]	Preprint, Jul	✗	✗	Generative Bbox	Implicit Search	NA	Low
Thyme-VL [50]	Preprint, Aug	✗	✗	Generative Code	Coarse-to-Fine	Coarse	High
DeepScan (Ours)	-	✓	✓	Hierarchical Scanning + Refocusing	Bottom-up	Hybrid	High

dus $r=20$. The IoU threshold for filtering similar evidence is $\theta_{IoU}=0.3$. We set $k=10$, *i.e.*, retain only the 10 smallest pairs $(b, e) \in \mathcal{E}$ for acceleration. For *Refocusing*, to prevent undersized crops, we pad the visual expert’s detections (\mathcal{B}) by 28 pixels on all sides, and set the scaling factor to $s=1.5$. For *LVLM Querying*, the maximum output length is 50 for *Evidence Decomposition*, *Evidence Judgment*, and *View Completeness Justification*, and 1024 for *Evidence-Enhanced Reasoning*. During inference, we use temperature $t=0$ with a fixed random seed (13). Beam search and top- k sampling are disabled by default.

Pseudocodes. Algorithmic details for Hierarchical Scanning and Refocusing are provided in Algorithms 1 and 2. Here, the prompts `Prompt1`, `Prompt2`, and `Prompt3` are specified in the **Prompt** subsection, *i.e.*, “User Prompt 1-3”; `Prompt1(x)` denotes instantiating the prompt with the string x via template-based substitution. In addition, `LIFTTOIMAGE` maps patch coordinates to the full-image coordinate system. `CLOSE` and `DILATE` indicate morphological closing and dilation, respectively. The operator \odot denotes element-wise multiplication.

C. Additional Results

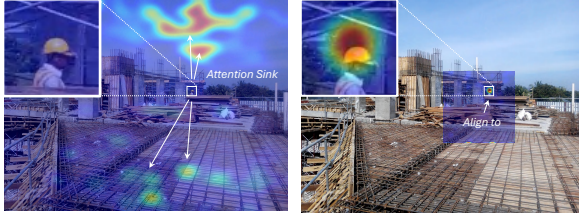
Baselines. SEAL [42], PixelReasoner [31], TreeVGR [35], DeepEyes [52], ViGoRL [28], and Thyme-VL [50] depend on learned localization modules or RL-based decision controllers for search. Upgrading these methods to a stronger LVLM typically requires retraining these components. In contrast, DyFo [13] performs MCTS over focus actions with a visual expert, and ZoomRefine [46] provides an unlearning variant that leverages LVLM prior for visually grounded reasoning through prompt engineering; both scale more readily across larger LVLM backbones. Our method is easier to scale up and introduces a novel bottom-up hierarchical scanning and refocusing for context-optimal views, complemented by a hybrid evidence memory, yielding bet-

Table 9. Additional comparison results on V* Bench between our method with existing baselines. We produced the results[†] with the provided official codes for fair comparisons.

	Overall	Attribute	Spatial
o3	95.0	-	-
Seal	74.8	76.3	75.4
Dyfo-L	62.7	53.9	59.2
Dyfo-Q	80.0	82.9	81.2
Qwen2.5-VL-7B	74.3	77.4	69.7
PixelReasoner	80.6	83.5	76.3
Thyme-VL	82.2	83.5	80.3
ZoomRefine [†]	82.2	85.3	77.6
Dyfo [†]	84.3	82.6	86.8
TreeVGR [†]	85.9	86.1	85.5
ViGoRL	86.4	-	-
DeepEyes	90.0	92.1	86.8
DeepScan ($k = 10$)	90.6	93.0	86.8
DeepScan ($k = \infty$)	91.1	93.9	86.8
Qwen2.5-VL-72B	84.8	90.8	80.9
DeepScan-72B ($k = 10$)	93.7	93.9	93.4
DeepScan-72B ($k = \infty$)	94.2	94.8	93.4

ter robustness than existing approaches.

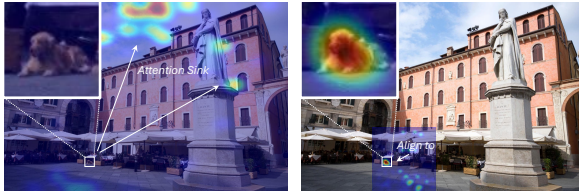
Performance Comparison. As shown in Table 9, **DeepScan** attains **90.6%** at $k=10$ and **91.1%** at $k=\infty$ based on Qwen2.5-VL-7B, which substantially outperforms both the training-free ZoomRefine[†] (82.2%) and DyFo[†] (84.3%) and even surpasses the RL-based DeepEyes (90.0%), ViGoRL (86.4%), TreeVGR (85.9%), Thyme-VL (82.2%), and PixelReasoner (80.6%) on the V* Benchmark. Specifically, on the *Attribute* subset, DeepScan reaches 93.0-93.9% while maintaining *Spatial* at 86.8%, indicating that bottom-up recovery plus refocusing preserves necessary



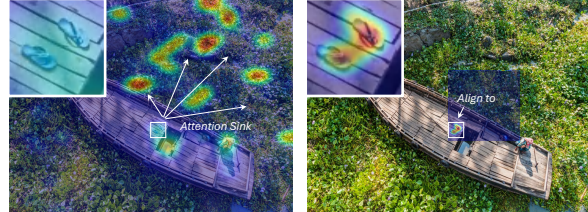
Q: What is the color of the **man's helmet**?



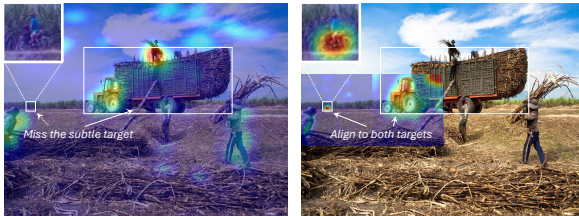
Q: What is the color of the **candles**?



Q: What is the breed of the **dog**?



Q: What is the color of the **slippers**?



Q: Is the **motorcyclist** on the left or right side of the **truck**?



Q: Is the **blue luggage** on the left or right side of the **bus**?



Q: Is the **sky wheel** on the left or right side of **the person on the horse**?



Figure 14. Qualitative analysis of the grounding paradigms with the attention map S of the *search expert*

context for reasoning. When scaling the LVLm backbone to 72B, **DeepScan-72B** achieves **94.2%** overall and 93.4% on the *Spatial* subset, a 9.4% gain over the Qwen2.5-VL-72B (84.8%). These results demonstrate DeepScan as a training-free framework that consistently improves diverse LVLms and benefits from model scaling, with a controllable performance-latency trade-off via top- k selection.

Engineering Optimization. Our standard implementation of DeepScan relies on nested loops using the *Hugging face transformers backend* (as detailed in Algorithms 1 and 2). However, this implementation is severely bottlenecked by inefficient **sequential computation** during the Scanning and Refocusing stages. Furthermore, the frequent communication overhead between the visual expert and the LVLm

leads to poor GPU utilization. Compounded by the *lack of modern primitives* in the standard **HF Transformers backend**, these factors result in substantial inference latency (as shown in Fig. 7). To address this, we introduce a suite of engineering optimizations that exploit DeepScan’s inherent algorithmic properties, significantly enhancing its viability for latency-sensitive applications. Specifically, unlike MCTS-based methods (e.g., Dyfo), DeepScan is built on *deterministic sampling*, enabling it to fully benefit from parallel acceleration via batching. Hence, we implemented batch processing for (a) attention map calculation, (b) top- k candidate judgment, and (c) evidence view justification, and further parallelized post-processing routines to reduce tail latency. This strategy compresses many sequential in-

	Qwen2.5-VL 7B	DeepEyes	Zoom Refine	Dyfo	Hierarchical Scan	Refocus	DeepScan
Accuracy (%)	75.4	89.0	82.7	83.8	84.8	89.5	90.1
Token Cost (k)	3.5	13	5.1	7.2	6.5	8.1	8.4
End-to-End Latency (s)	0.4	6.9	0.9	2.4	2.2	3.0	3.1

Table 10. Performance–efficiency comparison on V* Benchmark. *End-to-End* Latency is the wall-clock time *per sample* from input to final output, including all auxiliary steps (e.g., Evidence Decompositions, Expert Calls, Post-Processing, Evidence Judgments).

interactions into a *single batched* search expert call and *three* LVLN forward passes *with extended context*, thus *substantially improving GPU utilization and reducing GPU idle time*. Moreover, we migrated to the *vLLM backend*, leveraging PagedAttention and optimized CUDA kernels. *Collectively, these standard engineering optimizations yield an $\sim 8\times$ speedup over our previous implementation.*

Performance-Latency Trade-off. Integrating the above optimizations, we re-evaluated DeepScan via *VLMEvalKit* (with *vLLM* backend) on $4\times$ L20 GPUs. As shown in Table 10, compared to *DeepEyes* that relies on multi-turn tool executions, DeepScan exhibits striking superiority. Specifically, DeepEyes suffers a severe 6.9s latency and 13k token cost, while DeepScan attains higher accuracy (90.1% vs. 89.0%) with $\sim 2.2\times$ faster speed (3.1s) as well as $\sim 35\%$ fewer tokens. This reveals that batched deterministic sampling effectively bypasses the sequential overhead of agentic paradigms, yielding superior reasoning with higher efficiency. Against the MCTS-based method *Dyfo*, DeepScan also offers a favorable trade-off. It incurs a marginal latency overhead (3.1s vs. 2.4s) but delivers a substantial $+6.3\%$ accuracy gain. Notably, our *Hierarchical Scan* alone outperforms *Dyfo* (84.8% vs. 83.8%) with lower latency (2.2s).

In fine-grained scenarios, the target occupies a minuscule fraction of the image, resulting in an inherently low signal-to-noise ratio (SNR) where the effective visual signal is overwhelmed by context noise. In these cases, search-based methods struggle to identify a reliable initial anchor, frequently causing exhaustive tree expansion to degenerate into an inefficient random walk. By slicing the image and evaluating patches via a single batched forward pass, our hierarchical scan explicitly isolates the target, drastically amplifying the local SNR. Coupled with the subsequent *Refocus*—which requires merely 0.8s but yields a massive $+4.7\%$ performance leap—these results reveal a profound insight: systematically scaling compute to deterministically maximize visual SNR is fundamentally more efficient than heuristic search-tree expansion.

D. Additional Visualization

D.1. Qualitative Analysis of Grounding Paradigm

Direct Attributes. For attribute questions (e.g., helmet/slippers/candles color, dog breed), the *one-shot* variant tends

to lock onto globally salient but irrelevant regions, a typical *attention sink/drift* failure, yielding mis-localization or missing the true fine-grained cue. By contrast, our *bottom-up* paradigm begins with local cue exploration and iteratively recenters the view on the true evidence, effectively “pulling” attention back to the correct object—consistent with the figure’s transitions from *Attention Sink* to *Align to* on attribute examples. This behavior aligns with the paper’s analysis that top-down, one-shot localization is fragile under noisy context, whereas bottom-up scanning suppresses distractions and aligns attention with the correct target.

Spatial Relations. Relation questions (e.g., left/right of motorcyclist vs. truck, sky wheel vs. rider, blue luggage vs. bus) require jointly grounding *two* targets. The one-shot variant often fixates on a single salient object and *misses the subtle counterpart*, leading to incorrect relational judgments; bottom-up scanning progressively resolves and aligns to *both* entities, producing reliable spatial decisions—exactly reflected by the figure’s captions “Miss the subtle target / Miss one of the target” versus “Align to both targets.” Moreover, after evidence is recovered, *Refocusing* further calibrates the context window to an evidence-centric view, helping retain only the necessary surrounding context for reasoning.

D.2. Example Model Outputs

To illustrate the advantages of our approach, we present side-by-side qualitative examples comparing **DeepScan** with strong LVLNs—GPT-5 (run in its advanced reasoning mode), GPT-4o, and Qwen3-VL-235B-A22B—as well as training-free baselines *ZoomRefine* and *DyFo*. For a fair comparison across training-free methods, *ZoomRefine*, *DyFo*, and **DeepScan** all use Qwen2.5-VL-72B as the LVLN backbone. Each example reports both the visual grounding and the model’s answer. The following examples confirm that **DeepScan** delivers stronger visually grounded reasoning—superior evidence localization and more accurate answers—than the two representative training-free baselines. Moreover, **DeepScan** outperforms GPT-4o and the larger-scale Qwen3-VL-235B-A22B, despite using a smaller Qwen2.5-VL-72B backbone, in both perception and reasoning. Notably, its end-to-end inference latency is of the same order as GPT-5, indicating a favorable performance–efficiency trade-off.

Example 1

Images



Evidence

0.004%



GT

(A) white

Question: What is the color of the man's cap?
(A) white (B) blue (C) red (D) black

ChatGPT 4o ▾



What is the color of the man's cap? (A) white (B) blue (C) red (D) black

There is **no man visible in the image**, so the question "What is the color of the man's cap?" cannot be answered based on the provided photo. If you meant to upload a different image or if there's a specific region you'd like me to zoom in on or analyze further, please let me know!

📄 🌟 🗨️ 📶 🔄 ...

Qwen3-VL-235B-A22B 



What is the color of the man's cap? (A) white (B) blue (C) red (D) black

 **Qwen3-VL-235B-A22B**

Actually, **there is no man visible in the image**. The photo shows a landscaped outdoor area with palm trees, buildings (some beige, some blue), grass, and decorative pots — but **no people**, and therefore **no man wearing a cap**.

Since the question asks about “the man’s cap” but there is no man in the picture, **none of the options (A) white, (B) blue, (C) red, or (D) black can be correct**.

 **Correct Answer: None — there is no man in the image.**

If this is a test question, it may be designed to catch attention to detail — always check whether the subject actually exists in the image before selecting an answer.

Final Answer: Not applicable — no man present.

Images



Grounding Result



ZoomRefine Answer

Actually, there is no man visible in the image provided. The image shows a landscape with palm trees, buildings, grass, and a signpost, but no people. Therefore, there is no man's cap to determine the color of.

Predict Answer: N/A.



Question: What is the color of the man's cap? (A) white (B) blue (C) red (D) black

Images



Grounding Result



Dyfo Answer

The man in the image is wearing a cap. While the low resolution of the image makes it slightly ambiguous, the cap is definitively not white, blue, or red. It is a deep, dark shade that absorbs most of the light, which is characteristic of black. Therefore, the color of the man's cap is best identified as black.

Predict Answer: (D) black.



Question: What is the color of the man's cap? (A) white (B) blue (C) red (D) black

Images



Scanning Result



Refocusing Result



DeepScan Answer

The main body of the cap is a very light color, appearing as white or off-white against the darker, greenish background. Comparing the observed light color to the given options, the only option that matches the visual evidence is clearly white.

Predict Answer: (A) white.



Question: What is the color of the man's cap? (A) white (B) blue (C) red (D) black